Journal of ELECTRONIC MATERIALS, Vol. 41, No. 6, 2012
DOI: 10.1007/s11664-012-1955-3

Validating Steady-State and Transient Modeling Tools for High-Power-Density Thermoelectric Generators

D.T. CRANE,[1,2] C.R. KORIPELLA,[1] and V. JOVOVIC[1]

1.—Amerigon Inc., 5462 Irwindale Avenue, Irwindale, CA 91706-2058, USA. 2.—e-mail: dcrane@amerigon.com

Steady-state and transient models have been created in a MATLAB/Simulink environment for high-power-density thermoelectric generators (TEG). These numerical models, comprising simultaneously solved, nonlinear, energy balance equations, simulate novel TEG architectures, such as a cylindrical TEG with gas/liquid heat exchangers. Model validation studies, including component-level testing of thermoelectric (TE) subassemblies, interface thermal resistance tests, and full-scale TEG tests, were performed under different operating conditions and designs. Targeted finite-element analysis studies were also conducted. A full-scale cylindrical-shaped TE generator was built using high-power-density, segmented TE elements and tested on a test-bench with hot air and cold water with maximum power output of 608 W. Measured performance data from these tests were used in model validation. Process outlet temperatures, pressure drops, hot and cold shunt temperatures along the length of the TEG, TEG voltage, and TEG current are some of the performance variables included in the model validation. The validated model is now being used with more confidence to optimize new TEG designs for different applications.

Key words: Thermoelectric, power generation, model validation, waste heat recovery, steady state, transient

INTRODUCTION

There is an ongoing need to reduce the amount of energy that is used in the world. One way to reduce this usage is to recover the waste heat from many inefficient processes, including automotive propulsion, and convert the heat directly into electricity. Thermoelectrics (TE) have been shown to be a promising technology in the area of power generation and waste heat recovery technology. Specific design tools are needed to be able to most effectively design and optimize these TE systems. Considerable recent work has been conducted in the area of TE power generation and waste heat recovery modeling and model validation.[1–8] Much of this work has involved steady-state modeling of low-temperature ($<250°C$) devices using Bi_2Te_3 TE materials, and was done on simple couple-level or module-level devices or devices that use liquid heat exchangers on both sides of the device. This paper describes the validation of steady-state and transient models, introduced by Crane,[9] of a complex cylindrical-shaped thermoelectric generator (TEG) with hot gas and cold water heat exchangers. These numerical models, written in a MATLAB/Simulink environment, comprise simultaneously solved, nonlinear, energy balance equations, which are used to simulate novel TEG architectures, including cylindrical gas/liquid heat exchanger designs. The energy balance equations describe convective heat flow in the fluids, conductive heat flow through the heat exchangers, and conductive heat flow through the TE element subassemblies. The model uses a finite-volume approach with discretization in the axial direction of both hot and cold flows. The convective derivatives are calculated using first-order upwind or downwind differencing. Transverse or radial heat transfer is modeled using conduction equations with

(Received July 17, 2011; accepted January 21, 2012; published online February 24, 2012)

central differencing for the gradients. Each hot and cold section is separated into four control volumes. Differential algebraic equations simulate the energy balances for each control volume.

This model has been validated for both low-temperature (<250°C) Bi_2Te_3-only devices and devices operated at air inlet temperatures up to 620°C made of high-power-density, segmented TE material. The TEGs modeled and tested are cylindrical and have a gas medium on the hot side and a liquid medium on the cold side. Different aspects of the cylindrical design along with its benefits have been described and discussed extensively in previous papers[2,3,10–14] and will not be restated here. This paper describes component-level tests along with steady-state and transient empirical and simulated test results for the cylindrical TEG design with hot air and cold water heat transfer media.

COMPONENT-LEVEL MODELING

The foundation of a strong device model lies in the ability to test and capture the performance of the device's different components. In the TEG, these basic components include the hot- and cold-side heat exchangers and the TE subassemblies and their interfaces to the heat exchangers. The ability to predict the performance of the TE subassembly or building block is crucial in establishing the ability to model a complete TEG device. Model validation for low-temperature Bi_2Te_3 and medium-temperature segmented-material TE subassemblies has been previously reported.[2,3] However, this work was repeated here, since the shunt configurations and TE materials for the TE subassemblies have been changed in the current cylindrical TEG from previous TEG designs.[2,3,11,12]

Figure 1 shows measured versus simulated performance of TE subassemblies used in the cylindrical TEG devices. The first graph shows the results for a TE subassembly consisting only of Bi_2Te_3 TE elements. The second graph shows the results for a TE subassembly made of high-power-density, segmented TE elements consisting of half-Heusler (at the hot side) and Bi_2Te_3 (at the cold side). The difference between the simulated and measured power output is <5%. These tests were conducted at heater temperatures of 225°C and 430°C, respectively, and at water inlet temperature of 20°C. Component-level tests were performed on Bi_2Te_3 elements up to 300°C and up to 500°C for segmented TE elements at the hot end and up to 80°C at the cold end to understand the robustness of the subassemblies under temperature extremes and temperature cycling conditions.[3,14]

The hot shunts for the cylindrical TEG device are metal rings that surround the hot heat exchanger. A custom test setup was designed to characterize the thermal resistances of the electrically isolating layer on the cylinder and the thermal interface between this layer and the metal ring under high heat flux conditions similar to the TEG operating conditions.[15] Results from these tests were used to define the thicknesses and thermal conductivities (thermal resistances) of the interfaces in the model.

The cold shunt subassembly for the cylindrical TEG device is an innovative design with a complex geometry and heat flow path. Thermal grease connects the cold shunts and the cold tubes (cold-side heat exchanger). Since there are multiple parallel paths for the heat to travel on its way from the TE elements to the fluid in the cold tubes, the thermal resistance of this interface is difficult to model accurately. To confirm that the hot and cold shunts were being modeled correctly, a series of studies were conducted using finite-element analysis (FEA). Figure 2 shows an example picture from these analyses. The FEA simulations confirmed that the

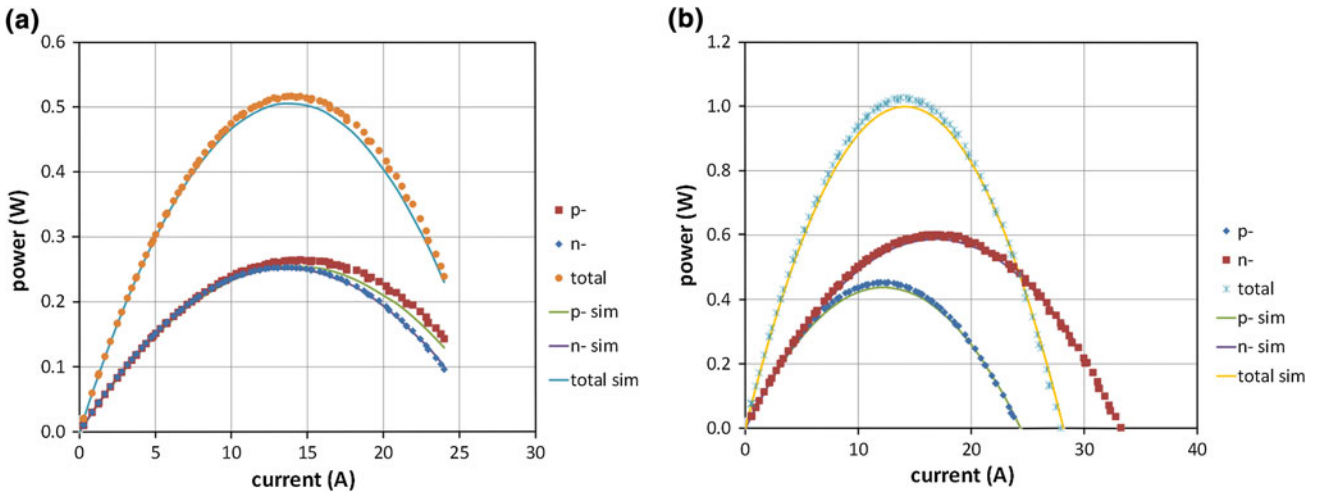

Fig. 1. Measured versus simulated performance of TE subassemblies made of Bi_2Te_3-only and segmented TE elements. The water temperature for both tests was 20°C. The heater temperature for the Bi_2Te_3-only test was 225°C. The heater temperature for the segmented TE element test was 430°C.

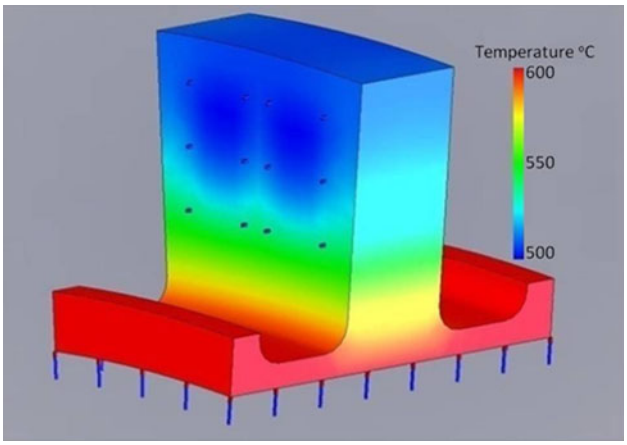

Fig. 2. FEA simulation results for the hot shunt.

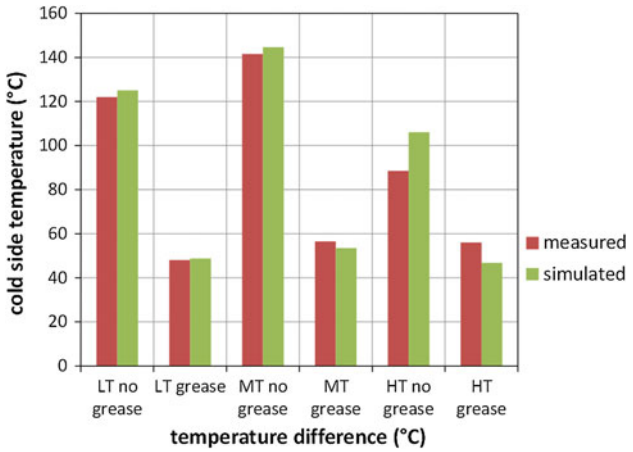

Fig. 3. Cold-side thermal grease and cold shunt thermal resistance study. Water temperature was 20°C. Grease thermal conductivity was 1.3 W/mK. Thermal conductivity without grease was 0.03 W/mK. Interface thickness was 0.03175 mm.

assumptions being used to model the hot and cold shunts and their thermal interfaces were correct.

Finite-element analysis and the related computational fluid dynamics (CFD) are very valuable tools in the design analysis of how the TEG device performs. FEA was also used in the design of the cylindrical TEG to determine the thermally induced stress on the hot rings/shunts. CFD was used to determine the flow uniformity of the cold fluid as it enters and exits the liquid manifolds. Flow uniformity is critical to understand if any sections of the TEG device will be coolant "starved" during operation. These tools were used in the design of various cylindrical TEG components. Further in-depth discussion of these topics is beyond the scope of this paper.

To further confirm the cold shunt subassembly model from a heat flow perspective, a series of tests were run on the TE subassemblies. These tests were designed to show the effect of thermal grease on the different temperature subassemblies and to demonstrate the ability to simulate the interfacial thermal resistance. Figure 3 shows a summary of these test results. LT, MT, and HT represent low-temperature, medium-temperature, and high-temperature TE subassemblies, respectively. These different TE subassemblies were used in separate sections of the TEG to better match the temperatures, temperature gradients, and heat fluxes in those areas of the TEG. Each of the three types of TE subassemblies was tested both with and without thermal grease in between the cold tube and cold shunt. Each subassembly was tested at the appropriate temperature conditions for that particular subassembly. Due to differences in the temperature gradient and thermal resistance of different TE elements, the heat flow across the thermal grease and into the cold tube was different for each subassembly. It can be seen from the graph that the thermal grease is important in keeping the temperature of the cold shunt as low as possible. Without thermal grease, the cold tube's ability to effectively sink rejected heat is limited. The agreement between the measured data and the model is within 10% for each of the three subassemblies both with and without thermal grease.

Additional component-level testing would normally be conducted on the hot- and cold-side heat exchangers independent of the TEG device itself. However, due to time and resource constraints, these tests were not done. The hot-side convective heat transfer coefficient and pressure drop correlations were taken from related empirical data, but still needed to be verified. The cold-side convective heat transfer coefficient and pressure drop correlations were taken from textbooks. These too would need to be verified for the particular configuration.

DEVICE-LEVEL STEADY-STATE TESTS AND MODEL VALIDATION

Using a similar modeling methodology, device-level steady-state model validation has been reported earlier for low-temperature (<250°C) TEG devices using single-material (Bi_2Te_3) elements with liquid heat exchangers in a planar configuration.[3] The error from measurement to model was <10%. The current version of the device-level steady-state model translates the planar construction of the previous model into a cylindrical design, first introduced by Bell and Crane.[11] Information obtained from the current component-level testing was integrated into the model. A Bi_2Te_3 low-temperature gas/liquid cylindrical TEG was built using the guidelines of this updated model. This device is shown in Fig. 4. Table I presents a list of tests run on the Bi_2Te_3 cylindrical TEG device. These conditions were meant to test the unit over a range of air and water inlet temperatures and flow rates. $T_{fh,in}$ and $T_{fc,in}$ represent hot and cold inlet temperatures, respectively, while $v_{dot,h}$ and $v_{dot,c}$ represent hot and cold volume flows.

Data from these 12 tests were then used to make modifications to the model to better simulate the actual TEG device. Despite the component-level testing described above, there is still uncertainty in many variables, particularly as they are scaled from the subassembly to the full-scale level.

As discussed earlier, the interface between the hot-side heat exchanger and the hot shunt/ring was studied previously. However, it was still uncertain how this interface would perform when its thermal resistance was averaged over many rings. It was also uncertain how this interface would perform when subjected to higher temperatures compared with the component-level tests. The interface between the cold-side heat exchanger (cold tube) and the cold shunt subassembly had similar uncertainty relating to how uniformly the thermal grease was applied across many cold shunts.

Uncertainty also existed in the average value of electrical interfacial resistance from the TE element to the hot and cold shunt. When stacking multiple TE subassemblies in series and in parallel, it is difficult to obtain the electrical interfacial resistance that can be obtained for a single TE subassembly. Although it is a goal to accurately measure the thermal interface resistance directly, as discussed in Crane,[9] the thermal interfacial resistance was calculated using the Wiedemann–Franz law. It became apparent from our component-level and initial device-level testing that this relationship did not hold for all situations, particularly as the electrical contact resistance increased. Thus, an additional Lorenz factor was included as a variable to be multiplied with the Lorenz number in the Wiedemann–Franz law.

$$\lambda = \frac{L_{\text{fact}} L T}{\rho}, \tag{1}$$

where L, the Lorenz number, is 2.45×10^{-8} (WΩ/K^2), T is the interface temperature (K), ρ is the electrical interfacial resistivity (Ω-m), λ is the thermal interfacial conductivity (W/mK), and L_{fact} is the Lorenz factor.

In an effort to reduce the number of variables, an overall average emissivity was used to predict the radiative heat transfer from each surface within the TEG. Emissivity is a material property that indicates the ability to emit heat radiatively from one surface to another compared with an ideal radiator. With so many different surfaces and surface finishes inside the TEG from the hot shunt to cold shunt to TE material, an average emissivity is difficult to predict. The emissivity of different materials can vary from low values of 0.05 up to values near unity depending on whether the surface has been oxidized or polished. Due to this uncertainty, average emissivity became another variable for which to solve. Included in this emissivity value is any uncertainty in view factor. In radiative heat transfer, view factor defines the amount of radiation that leaves one surface and intercepts another surface. Surfaces that are not in direct line of sight to the emitting surface may not see all of the emitted heat. For parallel plates, it is easy to determine the view factor or amount of radiative heat that it is possible to transfer from one parallel surface to another. The surfaces in the TEG device are not all parallel. Thus, there is some uncertainty in the amount of heat that is emitted by one surface and received by another. This value was included in the overall average emissivity. In the future, these terms can be broken down into more distinct variables to provide further simulation accuracy.

Finally, multipliers were included for four different heat transfer coefficients. Each coefficient was based on either general textbook correlations or empirical data for a similar component but not

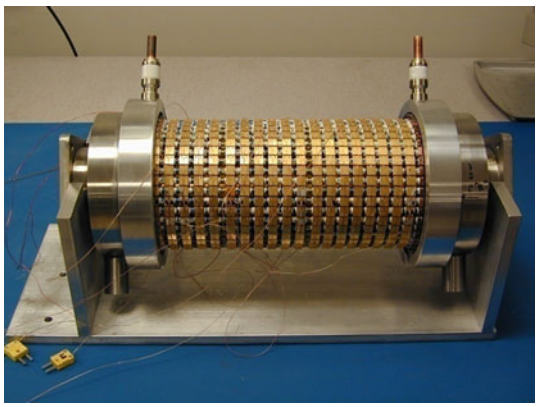

Fig. 4. Bi_2Te_3 cylindrical TEG device.

Table I. Test conditions for Bi_2Te_3 cylindrical TEG

Test	2	3	4	5	6	7	8	9	10	11	12	13
$T_{fh,in}$ (°C)	200	300	400	435	435	435	435	435	435	400	300	200
$T_{fc,in}$ (°C)	35	35	35	35	20	20	20	20	20	20j	20	20
$v_{dot,h}$ (cfm)	47	47	47	47	47	70	47	47	30	30	30	30
$v_{dot,c}$ (lpm)	15	15	15	15	15	15	10	20	15	15	15	15
Max. power output (W)	28.3	73.5	130	148	165	205	158	163	116	102	55.5	22.7

Note: Test 1 is not listed because it was only a water-side pressure drop test.

specific to the particular parts being tested. The heat transfer coefficients (W/m^2K) included the hot heat exchanger convection coefficient, h_{hot}, the cold heat exchanger convection coefficient, h_{cold}, free convection between the device and the environment, $h_{free,1}$, and free convection between the hot and cold sides of the device, $h_{free,2}$. The multipliers were used to adjust these correlations to better match the component performance in the actual device, see Eqs. 2–5.

Table II. Variable values used to provide least-squares fit to empirical test data

Variable	Value
Hot interface heat transfer coefficient (W/m^2K)	6562
Cold interface heat transfer coefficient (W/m^2K)	68,898
Electrical interfacial resistance ($\mu\Omega cm^2$)	65
Lorenz factor	65
Emissivity	0.4
Hot convective heat transfer coefficient multiplier	1.2
Cold convective heat transfer coefficient multiplier	1
Free convection multiplier 1	0.5
Free convection multiplier 2	1

$$Q_{conv,hot} = h_{hot} h_{mult,hot} A_{hot} (T_{f,hot} - T_{s,hot}), \quad (2)$$

$$Q_{conv,cold} = h_{cold} h_{mult,cold} A_{cold} (T_{s,cold} - T_{f,cold}), \quad (3)$$

$$Q_{free,1} = h_{free,1} h_{mult,free,1} A_s (T_{s,hot} - T_\infty), \quad (4)$$

$$Q_{free,2} = h_{free,2} h_{mult,free,2} A_s (T_{s,hot} - T_{s,cold}), \quad (5)$$

where Q is heat flow (W), h is heat transfer coefficient (W/m^2K), h_{mult} is the heat transfer coefficient multiplier, A is the heat transfer surface area (m^2), T is temperature (K), subscript "conv" is convective, subscript "hot" is for hot side, subscript "cold" is for cold side, subscript "f" is for fluid, subscript "s" is for surface, subscript "free" is for free convection, and subscript "∞" is for the environment.

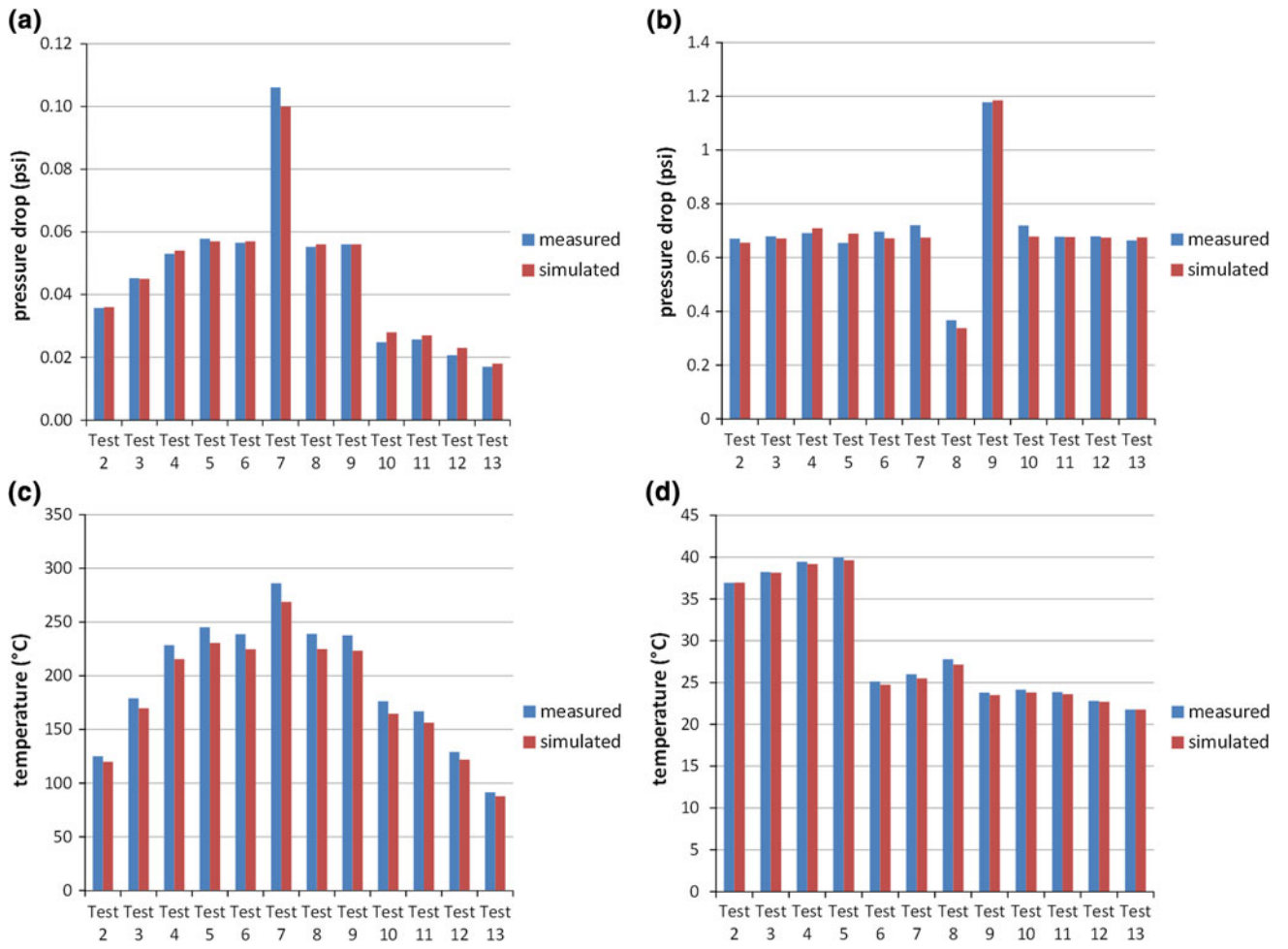

Fig. 5. Bi_2Te_3 cylindrical TEG test-bench results compared with simulated test results for TEG: (a) air pressure drops, (b) water pressure drops, (c) air outlet temperatures, and (d) water outlet temperatures.

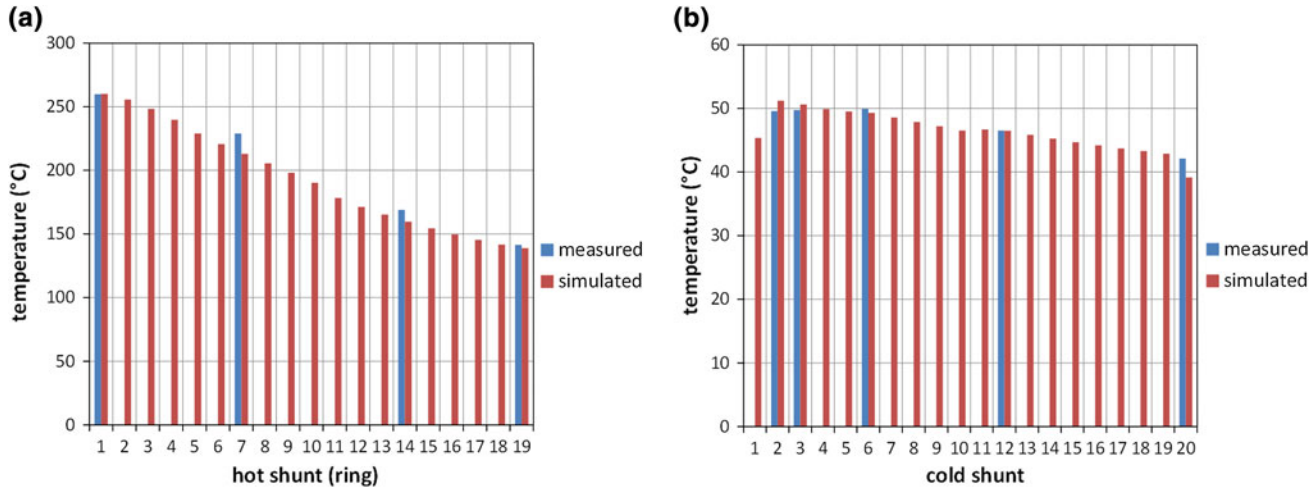

Fig. 6. Bi_2Te_3 cylindrical TEG test-bench results compared with simulated test results for TEG: (a) hot shunt temperatures and (b) cold shunt temperatures. Data for test 5 at peak current.

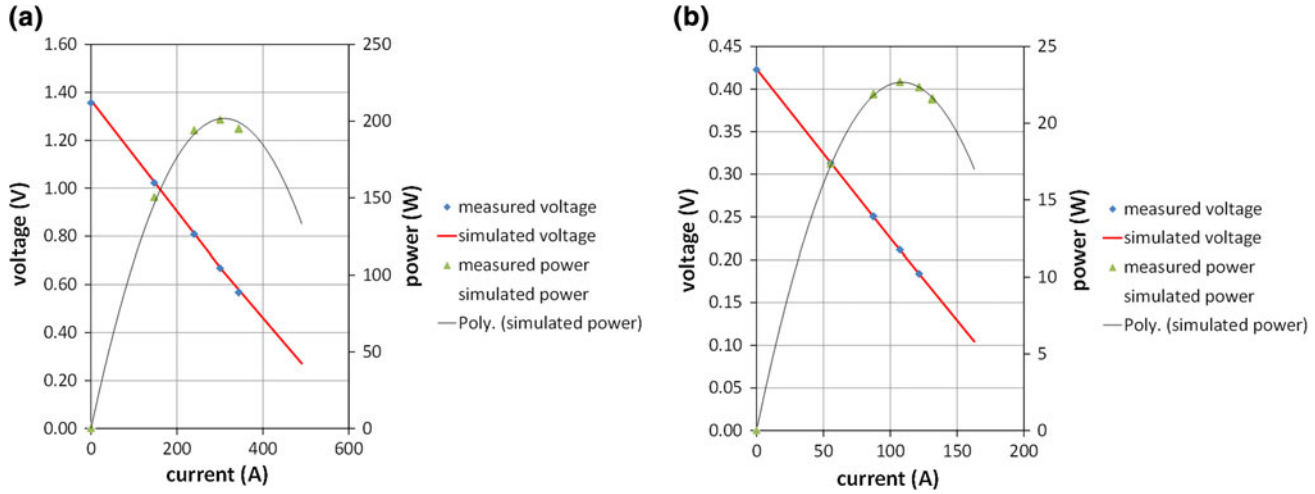

Fig. 7. Bi_2Te_3 cylindrical TEG test-bench results compared with simulated test results for TEG voltage and power output: (a) test 7 and (b) test 13.

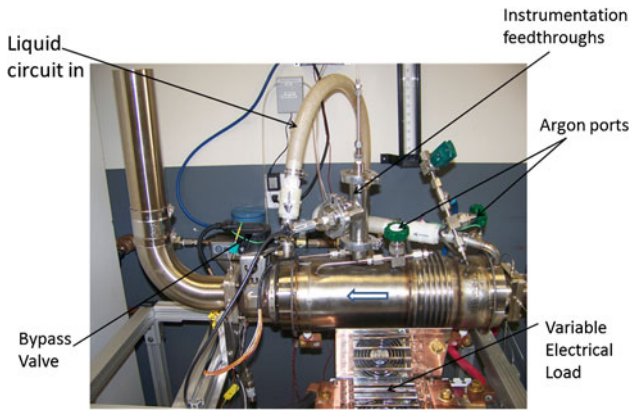

Fig. 8. Medium-temperature TEG on the test-bench.

Simulations were then run using these variables, allowing them to vary to create a least-squares or best fit to the data. Table II lists the variables along with the values that provided the best fit to the data. All of these values are reasonable and not outside the range that is physically possible.

Figure 5 shows the empirical test results of tests 2 to 13 compared with simulated test results for air and water pressure drop and outlet temperatures. The difference between the measured and simulated values is $<5\%$. For the air outlet temperature, the difference is slightly higher, but in this case there is also some uncertainty in the air temperature measurements due to stratification of temperature within the air flow within the pipe. Three thermocouples were used to try to measure

Table III. Test conditions for medium-temperature cylindrical TEG made of segmented TE material

Test	1	2	3	4	5	6	7	8	9	10	11	12
$T_{fh,in}$ (°C)	390	390	390	425	425	425	510	510	510	620	620	620
$T_{fc,in}$ (°C)	20	20	20	20	20	20	20	20	20	20	20	20
$m_{dot,h}$ (g/s)	13.5	13.5	13.5	20.5	20.5	20.5	30.1	30.1	30.1	45	45	45
$m_{dot,c}$ (g/s)	170	250	330	170	250	330	170	250	330	170	250	330
Max. power output (W)	56.1	56.5	57.6	119	121	122	261	270	272	495	580	595

Test	13	14	15	16	17	18	19	20	21	22	23	24	25
$T_{fh,in}$ (°C)	390	390	390	425	425	425	510	510	510	620	620	620	620
$T_{fc,in}$ (°C)	40	40	40	40	40	40	40	40	40	40	40	40	20
$m_{dot,h}$ (g/s)	13.5	13.5	13.5	20.5	20.5	20.5	30.1	30.1	30.1	45	45	45	48
$m_{dot,c}$ (g/s)	170	250	330	170	250	330	170	250	330	170	250	330	330
Max. power output (W)	49.3	49.2	49.6	103	104	106	228	237	241	436	461	N/A	608

Note: Test 24 not completed due to chiller overheating.

Table IV. Variable values used to provide least-squares fit to empirical test data

Variable	Value
Hot interface heat transfer coefficient (W/m^2K)	20997
Cold interface heat transfer coefficient (W/m^2K)	39370
Electrical interfacial resistance ($\mu\Omega cm^2$)	25.0, 17.5, 13.5
Lorenz factor	25.0, 17.5, 13.5
Emissivity	0.58
Free convection multiplier 1	1.75
Free convection multiplier 2	1.75

the outlet air temperature in different parts of the airstream. Using more thermocouples and/or a temperature integrator would potentially further reduce the error between measured and simulated data for air outlet temperature.

Figure 6 shows a comparison between measured and simulated data for hot and cold shunt temperatures in the TEG for test 5. Similar graphs were achieved for all of the different test conditions. Again, there is excellent correlation between the simulated and measured results down the axial length of the TEG (from hot ring 1 to 19, from hot air inlet to outlet).

Figure 7 shows the measured versus simulated voltage and power output for tests 7 and 13. Similar graphs were achieved for all of the different test conditions. Again, we can see excellent correlation between measured and simulated data. The difference between the measured and simulated data is $<5\%$ across the range of electrical currents for both test conditions.

In addition to the low-temperature cylindrical TEG, a medium-temperature gas/liquid cylindrical TEG was built and tested, as shown on the test-bench in Fig. 8. This device differed from the low-temperature TEG. It was made of segmented TE material, half-Heusler and Bi_2Te_3. It was also operated at higher temperatures, requiring it to operate in an inert environment (argon) to prevent oxidation of the TE elements and the hot shunts. To ensure the inert environment, an outer shell was added to the device as can be seen in Fig. 8. The figure also shows the argon ports used to establish the inert environment and the instrumentation feedthroughs. A bypass valve, shown in the figure, is also a part of this construction to allow high-temperature, high-flow gas to bypass the TEG.

Similarly to the low-temperature TEG, Table III presents the list of tests run on the medium-temperature cylindrical TEG device. These conditions were again meant to test the unit over a range of air and water inlet temperatures and flow rates.

The results of the Bi_2Te_3 TEG testing became inputs for the segmented TE material device. The hot and cold convective heat transfer coefficient multipliers were fixed to the values for the Bi_2Te_3 TEG and were no longer used as variables for the least-squares fit of data. Table IV lists the best fit values for the medium-temperature TEG.

The emissivity and free convection multipliers changed as the materials changed from the Bi_2Te_3 to the medium-temperature TEG. The addition of the outer shell also affected these parameters. The hot interfacial resistance became lower because the interfacial resistance is a function of the hoop stress between the metal shunt/ring and the stainless-steel (SST) heat exchanger. The hoop stress increases as a function of temperature. The cold interface became worse due to variations in manufacturing tolerances. The electrical interfacial

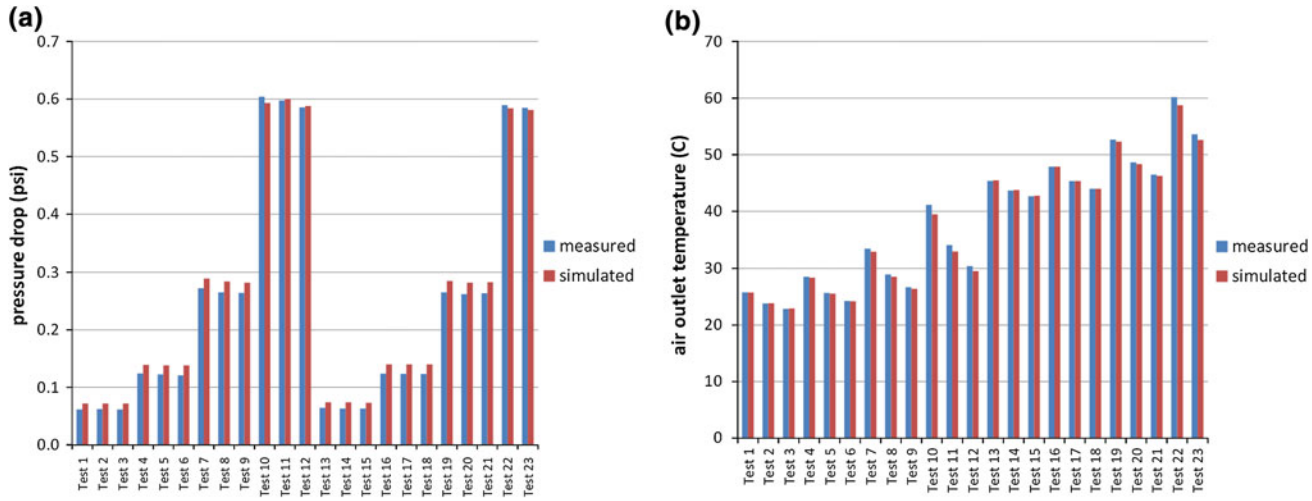

Fig. 9. Medium-temperature cylindrical TEG test-bench results compared with simulated test results for TEG: (a) air pressure drops and (b) water outlet temperatures.

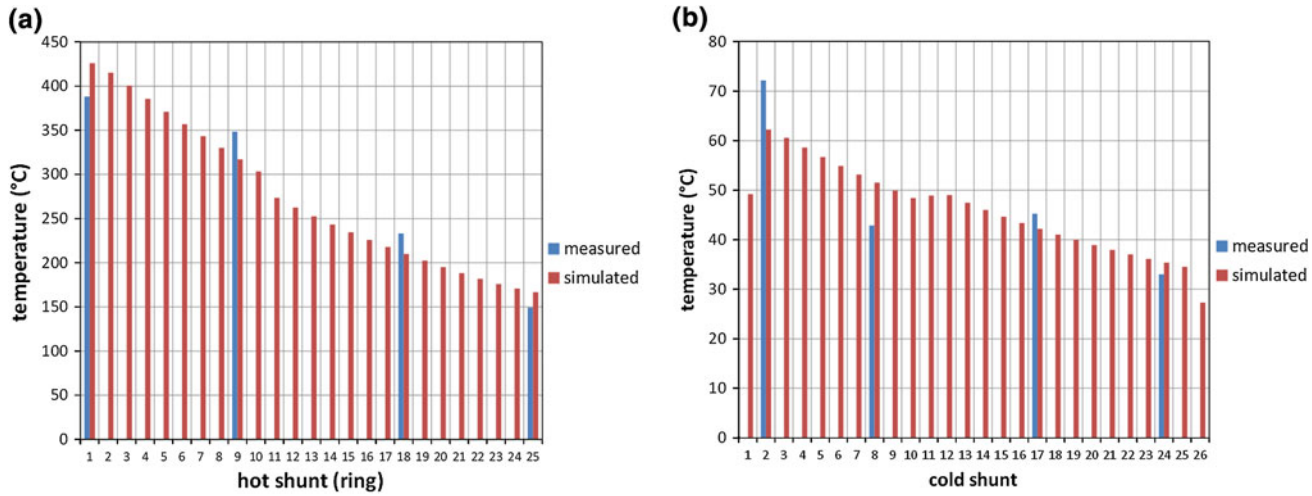

Fig. 10. Medium-temperature cylindrical TEG test-bench results compared with simulated test results for TEG: (a) hot shunt temperatures and (b) cold shunt temperatures. Data for test 11 at peak current.

resistance and Lorenz factors improved over the Bi_2Te_3 unit due to differences in TE materials and TE material interfaces. These variables also decreased as the device was tested further. This is thought to be caused by an annealing effect on the interfaces that results from thermal cycling. This has also been seen in thermal cycling results at the TE subassembly level. The electrical interfacial resistance went from 25 $\mu\Omega cm^2$ to 17.5 $\mu\Omega cm^2$ after the device was taken to 620°C air inlet temperature. The electrical interfacial resistance went from 17.5 $\mu\Omega cm^2$ to 13.5 $\mu\Omega cm^2$ after the chiller overheated and shutdown, causing the cold shunt temperatures to increase to over 120°C.

Figure 9 shows the empirical test results of tests 1 to 24 compared with simulated test results for air pressure drop and water outlet temperatures. The difference between the measured and simulated values is $<5\%$. Again for air outlet temperature (not shown), the difference is $>10\%$, but this measured value has significant error itself due to stratification of temperature within the air flow, which is a function of air inlet temperature and air flow.

Figure 10 shows a comparison between measured and simulated data for hot and cold shunt temperatures in the TEG for test 11. Similar graphs were achieved for all of the different test conditions. There is slightly more error in these results than the error shown in the previous results for the Bi_2Te_3 TEG. This is due to error in surface contact temperature measurements.

Figure 11 shows the measured versus simulated voltage and power output for tests 11 and 19. Similar graphs were, again, achieved for all of the

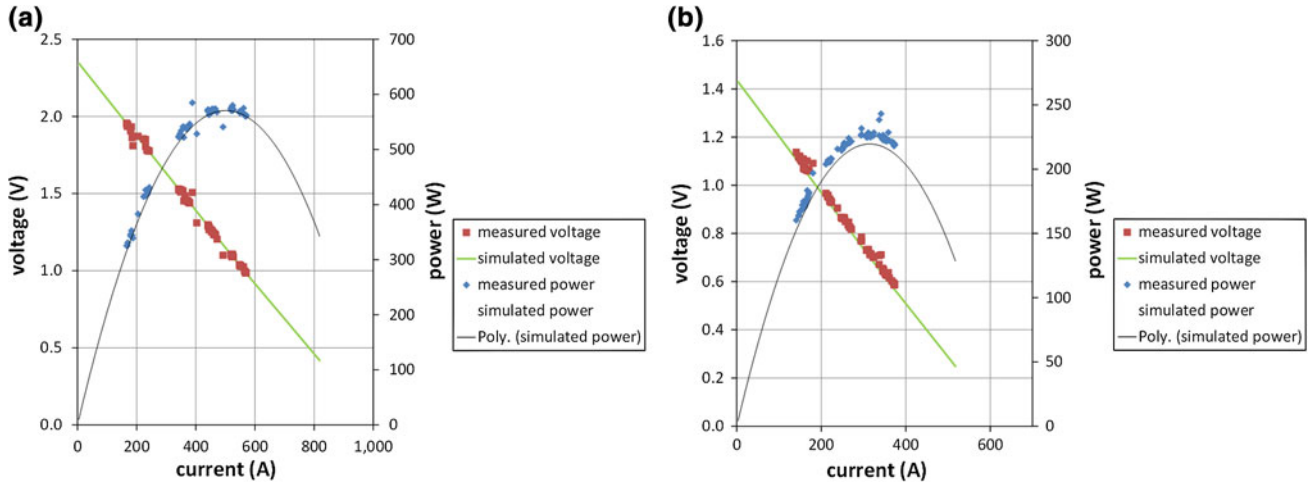

Fig. 11. Medium-temperature cylindrical TEG test-bench results compared with simulated test results for TEG voltage and power output: (a) test 11 and (b) test 19.

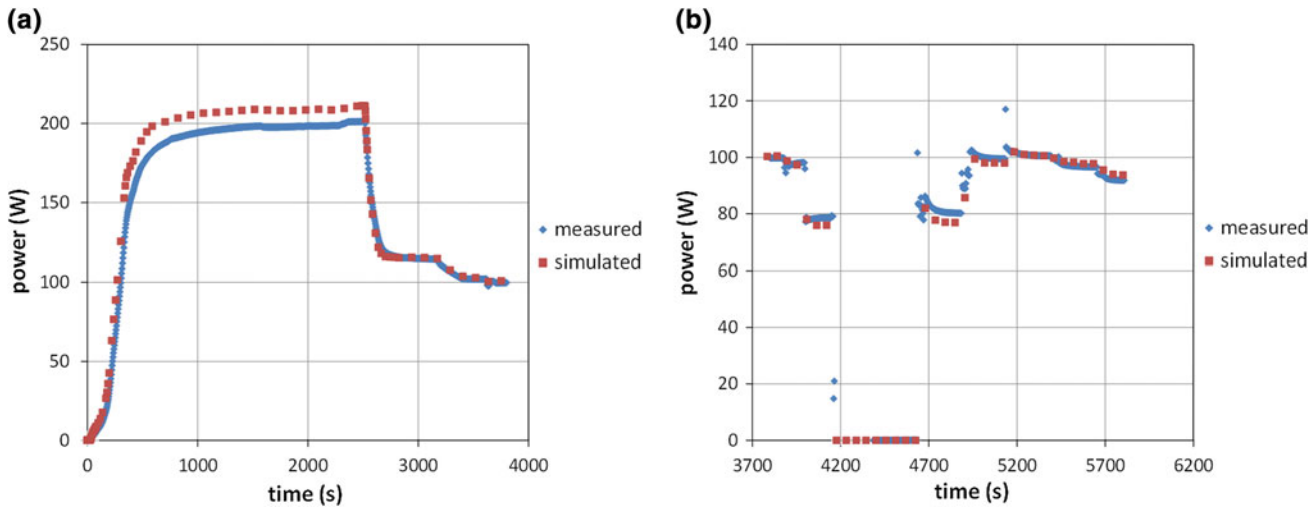

Fig. 12. Transient test results for Bi_2Te_3 cylindrical TEG compared with simulated transient results for: (a) changing hot and cold temperatures and flows, and (b) changing electrical load.

different test conditions. Error between measured and simulated data is $<5\%$ across the range of currents for both test conditions.

Maximum power achieved on the test-bench for this TEG was 608 W in test 25 as shown in Table III. This corresponds to power density of 42 W/L (based on flange-to-flange dimension including outer shell and internal bypass) and 1100 W/kg of TE material used.

DEVICE-LEVEL TRANSIENT TESTS AND MODEL VALIDATION

With the steady-state device-level model validated for a range of conditions and designs, this model can now be used as the starting point for transient device-level model validation. Additional component-level tests were not conducted with the exception of the transient TE couple tests described in Crane.[9] The good agreement in these transient couple tests in response to a sudden change in electrical load resistance is another important building block towards the transient device-level model. Transient response of the cold tubes and the hot-side heat exchanger could have been tested and would certainly have helped in the validation process.

Figure 12 shows the measured and simulated transient response of the Bi_2Te_3 TEG. The first graph shows the transient response of the TEG as the hot- and cold-side temperatures and flows vary. The slight difference in this graph is due to the error in the steady-state model.

The second graph shows the transient response to changes in electrical load resistance on the TEG. This load resistance goes from open circuit to other resistances including the load resistance at peak

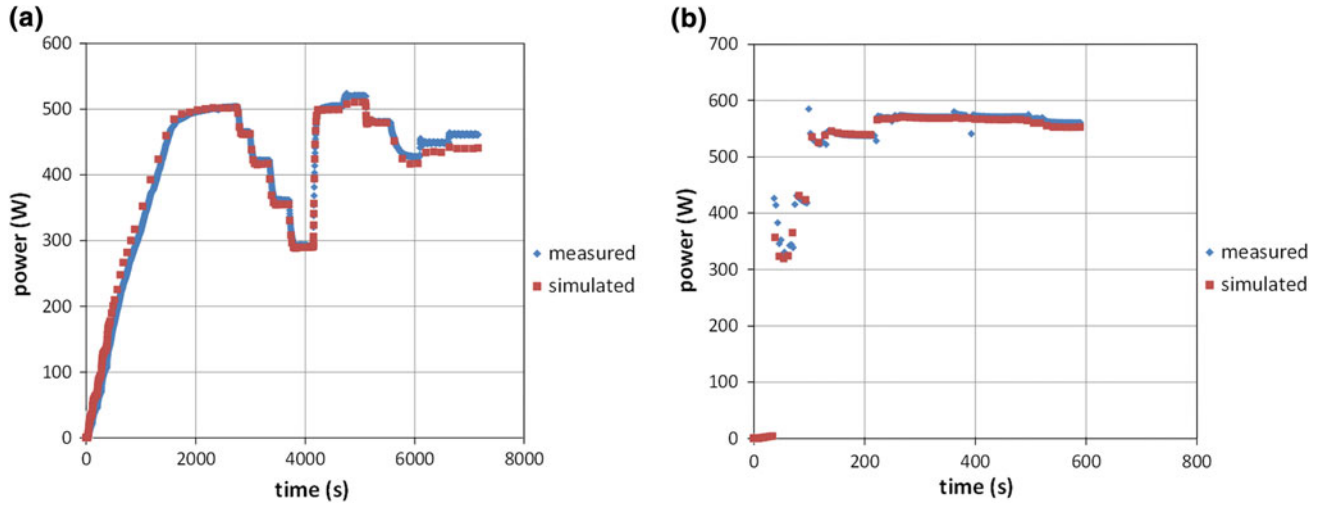

Fig. 13. Transient test results for medium-temperature cylindrical TEG compared with simulated transient results for: (a) changing hot and cold temperatures and flows, and (b) changing electrical load.

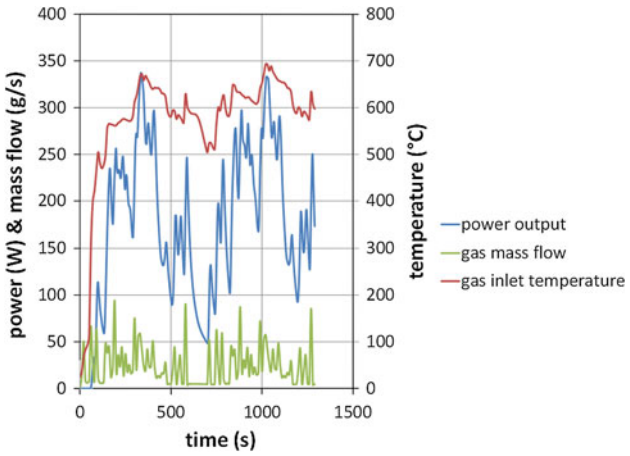

Fig. 14. Simulated TEG performance for the US06 drive cycle. The cold inlet temperature was 80°C, and the cold flow was 250 g/s.

power. All of the other operating conditions were held constant for this graph. It can be seen from these graphs that agreement between the measured and simulated data is very good. The model captures the sudden changes in temperature, flow, and load resistance. Figure 13 shows similar graphs for the medium-temperature TEG.

With the transient model of the cylindrical TEG device having been validated, it is now possible to run drive cycle simulations with more confidence in the output. Figure 14 shows the results from such a simulation.

CONCLUSIONS

The steady-state and transient models for a gas/liquid cylindrical TEG first introduced in Crane[9] have been validated. Process outlet and shunt temperatures along with pressure drops, voltage, and power output all vary by $<10\%$ between the measured and simulated values for a range of process conditions and across two different TEGs made of different TE materials.

The validated model has been applied with more confidence to new transient simulations for the US06 drive cycle to show estimated TEG performance over such a cycle.

The medium-temperature TEG is currently being installed in a BMW X6. Once installed, further test results will be available to compare against simulated data at the device and vehicle levels. A third TEG is also being built to the same specifications as the medium-temperature TEG and will be compared against the reported TEG for reproducibility. This TEG will be tested on a dynamometer at the National Renewable Energy Laboratory (NREL) and then be installed and tested on a Ford Fusion.

With the steady-state model validated, it can now be used with more confidence with optimization algorithms[9] to improve designs and support the continued path towards commercialization. A very powerful set of validated tools has been created that will greatly aid in the design of future TE power generation devices and systems.

ACKNOWLEDGEMENTS

The author would like to thank John Fairbanks and the US Department of Energy Office of Vehicle Technologies for their support and funding for much of the work relating to this paper; Carl Maronde from DOE NETL for program management; Andreas Eder and Boris Mazar from BMW and Clay Maranville from Ford for their valued support as program team leaders; John LaGrandeur from Amerigon for his overall program management and support; Steve Davis and Dmitri Kossakovski from Amerigon for their support and leadership; the rest of the Amerigon team for all of their hard work in completing this paper; the Faurecia team for their

contributions in building the TEGs; and Lon Bell for his overall consultation and inspiration without which this work could not have been completed.

REFERENCES

1. D.T. Crane, *Optimizing Thermoelectric Waste Heat Recovery from an Automotive Cooling System* (College Park, MD: University of Maryland, College Park, 2003).
2. D.T. Crane, D. Kossakovski, and L.E. Bell, *J. Electron. Mater.* 38, 1382 (2009).
3. D.T. Crane, J.W. LaGrandeur, F. Harris, and L.E. Bell, *J. Electron. Mater.* 38, 1375 (2009).
4. N. Espinosa, M. Lazard, L. Aixala, and H. Scherrer, *J. Electron. Mater.* 39, 1446 (2010).
5. M. Chen, S.J. Andreasen, L.A. Rosendahl, S.K. Kaer, and T. Condra, *J. Electron. Mater.* 39, 1593 (2010).
6. X.L. Gou, H. Xiao, and S.W. Yang, *Appl. Energy* 87, 3131 (2010).
7. Y.Y. Hsiao, W.C. Chang, and S.L. Chen, *Energy* 35, 1447 (2010).
8. D. Ebling, M. Jaegle, M. Bartel, A. Jacquot, and H. Bottner, *J. Electron. Mater.* 38, 1456 (2009).
9. D.T. Crane, *J. Electron. Mater.* 40, 561 (2011).
10. L.E. Bell, *23rd International Conference on Thermoelectrics* (Adelaide, Australia, 2004).
11. L.E. Bell and D.T. Crane, *International Thermoelectric Conference* (Freiburg, Germany, 2009).
12. D.T. Crane and L.E. Bell, *25th IEEE International Conference on Thermoelectrics* (Vienna, Austria, 2006).
13. D.T. Crane and L.E. Bell, *J. Energy Resour. ASME* 131, 012401 (2009).
14. D.T. Crane, J.W. LaGrandeur, and L.E. Bell, *J. Electron. Mater.* 39, 2142 (2010).
15. C.R. Koripella, L.E. Bell, D.T. Crane, and D. Wang, *MRS Spring Meeting* (San Francisco, CA, 2011).